Journal of MATERIALS RESEARCH

Article
DOI:10.1557/s43578-021-00250-1

ADVANCED NANOCATALYSTS FOR ELECTROCHEMICAL ENERGY STORAGE AND GENERATION

Check for updates

FOCUS ISSUE

Effect of the oxidation state and morphology of SnO_x-based electrocatalysts on the CO_2 reduction reaction

Lara G. Puppin[1], Luís F. da Silva[2], Marcelo Carmo[3], Hamilton Varela[1], Osmando F. Lopes[1,3,4,a)]

[1] São Carlos Institute of Chemistry, University of São Paulo, 780, São Carlos, SP 13560-970, Brazil
[2] Laboratory of Nanostructured Multifunctional Materials, Federal University of São Carlos, São Carlos, SP 13565-905, Brazil
[3] Institute of Energy and Climate Research: Electrochemical Process Engineering (IEK-14), Forschungszentrum Jülich GmbH, 52425 Jülich, Germany
[4] Laboratory of Photochemistry and Materials Science, Institute of Chemistry, Federal University of Uberlândia, Uberlândia, MG 38400-902, Brazil
[a)] Address all correspondence to this author. e-mail: osmando_iq@hotmail.com

Received: 6 January 2021; accepted: 15 May 2021; published online: 1 June 2021

CO_2 electrochemical reduction reaction (CO_2RR) is an attractive strategy for closing the anthropogenic carbon cycle and storing intermittent renewable energy. Tin-based electrocatalysts exhibit remarkable properties for reducing CO_2 into HCOOH. However, the effects of morphology and oxidation state of tin-based electrocatalysts on the performance of CO_2 reduction have not been well-described. We evaluate the oxidation state and particle size of SnO_x for CO_2 reduction. SnO_x was effective for converting CO_2 into formic acid, reaching a maximum selectivity of 69%. The SnO exhibited high activity for CO_2RR compared to SnO_2 electrocatalysts. A pre-reduction step of a SnO_2 electrocatalyst increased its CO_2 reduction performance, confirming that Sn^{2+} is more active than Sn^{4+} sites. The microsized SnO_2 is more effective for converting CO_2 into formic acid than nanosized SnO_2, likely due to the impurities of nanosized SnO_2. We illuminated the role played by both SnO_x particle size and oxidation state on CO_2RR performance.

Introduction

Global energy consumption is highly dependent upon fossil fuels, and climate models have shown that CO_2 emissions are inducing climate change due to the greenhouse effect [1, 2]. The conversion of CO_2 into valuable chemicals and fuels by means of electrochemical reduction could solve both the environmental and energy crises [2–4]. This process carries several advantages, such as low-temperature operation, that it can be run at ambient pressure, and the required energy input can be supplied from renewable energy sources (i.e., solar or wind), creating a net-zero CO_2 emission condition in certain energy business cases [5–7]. Moreover, the performance and selectivity of such an electrochemical reaction can be tuned, and the scale-up of this process becomes simpler than other such as: photochemical and thermochemical process [8–10].

The CO_2 reduction reaction (CO_2RR) is a multielectron process that may proceed via different reaction pathways, yielding diverse reduction products, such as CO and HCOOH (2 electrons), CH_3OH (6 electrons), CH_4 (8 electrons), C_2H_4 (12 electrons) depending on the electrocatalysts and experimental conditions [11]. Formic acid has been receiving significant attention as an CO_2RR product due to its stability, remarkably high volumetric capacity, and its versatile potential use in various applications (*e.g.*, direct formic acid fuel cells, and the leather, textile, food, and chemical industries) [12, 13]. The economic viability of various chemicals from the CO_2RR demonstrated that formic acid has a great business value, which is one of the most desired products [10]. However, the inertness of CO_2 due to its high chemical stability results in a process with high overpotential, sluggish kinetics, and broad distribution of products [3, 14, 15]. The physical–chemical properties of an electrocatalyst, such as morphology [16], chemical state [17–19], and surface features strongly depend on its CO_2RR performance. Therefore, rationalizing the effect of each catalyst's properties on CO_2 reduction is especially important in the development

© The Author(s) 2021

of new kind of materials to overcome the major challenges in this field [20].

Among the materials for converting CO_2 into formic acid, tin (Sn)-based ones exhibit remarkable features, such as good selectivity, low costs, and nontoxicity [21–24]. However, bare Sn planar electrodes present a current density of – 5 mA cm^{-2} with 80% Faradaic efficiency and an overpotential of almost 0.90 V, which is too low for practical applications [25]. The role played by metal semiconducting oxide, oxidation state and morphology whether as catalysts for the formation of oxygenates, still remains unclear [18, 26, 27]. Some researchers have shown that a layer of metal oxide on the catalyst surface can decrease the reaction overpotential and increase the performance of the CO_2RR [18, 26–29]. Additionally, Kanan et al. [28] demonstrated that the removal of the SnO_x native layer from an Sn electrode results in near exclusive H_2 evolution activity. It was also demonstrated that CO_2RR performance of SnO_x-based electrocatalyst decreased after Sn^{4+} reduction to Sn^0, they verified the occurrence of three processes: CO_2 reduction into formic acid, hydrogen evolution reaction and the reduction of the SnO_2 catalyst which yields tin species of lower oxidation number (that is, Sn^0 and probably Sn^{2+} species as well) [27]. Additionally, at moderately cathodic potentials, SnO_2 exhibited high selectivity for the production of formate, while at very negative potentials it was observed the reduction of oxide to Sn, and the efficiency of formate production was significantly decreased [27]. Therefore, Sn-based catalysts showed low stability during long periods of operation, as the reduction of SnO_x species in Sn metallic decreases its activity [28, 30]. However, it has also been found that the deposition of electrocatalysts on carbon paper can increase its performance and stability [31, 32]. Nevertheless, SnO_x-based nanoparticles deposited on carbon paper have thus far been little explored for CO_2 reduction applications.

This manuscript reports on a series of evaluations of the effect of tin oxidation states, as well as the particle size of SnO_x deposited on carbon fiber on CO_2RR activity and selectivity. Additionally, the electrocatalyst's stability was also assessed by means of physicochemical characterization of the electrodes before and after the CO_2RR experiments. Finally, the influence of the reduction potential was evaluated in terms of CO_2RR performance and the stability of SnO_x-based materials.

Results and discussion

XRD patterns of the SnO_x-based electrodes (Fig. 1) were obtained to confirm the presence of SnO_x material and crystalline phase on carbon paper electrode, for comparison purposes the XRD patterns of the pristine materials were also obtained (Figure S1). All of the electrodes exhibited an identical crystalline phase before and after deposition onto carbon fiber, indicating that the method proposed was effective for impregnating

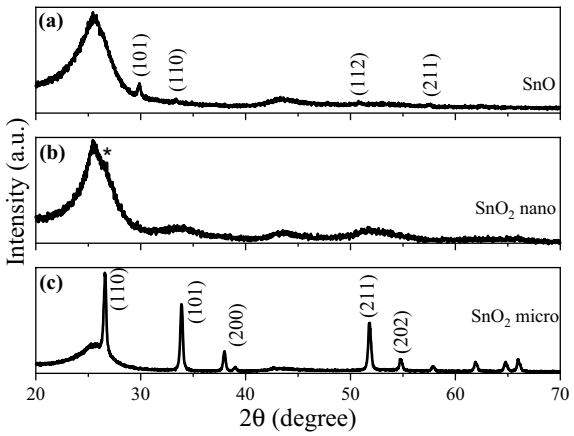

Figure 1: XRD patterns of SnO_x (microsized and nanosized) deposited onto carbon fiber with all reflection peaks indexed.

the SnO_x materials. All of the electrodes exhibited a broad peak at about 26° that could be related to the carbon fiber [13]. SnO (PDF2: 01-172-1012) exhibited small peaks due to the small amount in the carbon fiber (18 mg); however, its characteristic peaks related to the plane (101) could be observed. Microsized SnO_2 exhibited all peaks in a well-defined way; on the other hand, as expected, nanometric SnO_2 exhibited small and broad peaks due to its small particle size [33]. In addition, the main peak from SnO_2, i.e., the (101) plane was overlapped by a carbon fiber peak of about 26°. The material's crystallite size was estimated from the XRD pattern using Scherrer equation (Table SI). It can be seen that SnO and SnO_2 microsized exhibited a crystallite size value of ca. 43 and 45 nm, respectively. On the other hand, the SnO_2 nanosized exhibited a crystallite size of ca. 5 nm. The results are in agreement with the material's morphology. Therefore, the XRD results confirmed that the electrode fabrication method was efficient to obtain the SnO_x electrodes without crystalline phase modification.

SEM images of the electrodes revealed that SnO_x particles were successfully deposited on the carbon fiber, as can be seen in Figure S2. The formation of agglomerated spherical particles attached to the carbon fibers can also be observed, such a feature becomes deleterious in catalytical applications [34, 35]. However, it can be seen that the carbon fiber was not entirely covered by the SnO_x particles, and this feature could aid in CO_2 reduction processes using oxide-based materials. It was demonstrated that a complete recovery of carbon fiber or electrode by a semiconductor can be deleterious for electrocatalytic performance, as it increases the electrode resistance, thus hampering the charge transfer processes [13]. Nanosized SnO_2 electrode seems more homogeneous than the microsized SnO_2 and SnO, it is likely related to the lower particle size and higher specific surface area that will be easier spread on the carbon fiber. Additionally, the specific surface area of the pristine materials was determined

© The Author(s) 2021

applying the BET model to N_2 physisorption data. SnO_2 nanosized material exhibited a SSA value at least 30 times higher than the SnO_x microsized materials, as can be seen in the Table SI. This result is in agreement with the materials morphologies.

Cyclic voltammetry was performed on the SnO_x-based electrodes to identify the reduction potential of the CO_2 reduction reaction, the hydrogen evolution reaction, and for SnO_x redox (Fig. 2). All of the electrodes exhibited two coinciding anodic peak in the potential region between 0.1 and − 0.1 V, and this was associated with the oxidation of Sn metallic to Sn^{2+} and Sn^{+2} to Sn^{+4}, even in SnO_2 electrodes, which is likely due to in situ reduction of Sn^{4+} to Sn^{2+} and Sn metallic during cathodic sweeps. The enlarged cyclic voltammetry of microsized SnO_2 exhibited two anodic peaks at − 0.13 V and + 0.01 V (Figure S3a), while the microsized SnO exhibited two peaks at − 0.06 V and + 0.05 V (Figure S3b). These peaks can be attributed to two different oxidation steps, the first one could be related to the oxidation of Sn to Sn^{2+}, while the second one could be related to the oxidation of Sn^{2+} to Sn^{4+} [21, 22, 36, 37].

The micrometric SnO_2 exhibited the highest current density at − 1.0 V, followed by the SnO and nanometric SnO_2 electrode, respectively. It was unexpected, because the material with a lower particle size and higher specific surface area should exhibit the higher electrochemical active surface area and, consequently, a higher current density. The reasons of the low activity of nanosized SnO_2 was investigated by X-ray photoelectron spectroscopy (Figure S4). The survey spectrum confirms the presence of Sn, O, C, and Cl. Note that, the presence of the elements Sn and O is in accordance with the composition and chemical state of the SnO_2 nanosized. The peaks related to carbon are from adventitious contamination commonly used as a charge reference for XPS spectra. The peak at 199.0 eV can be attributed to Cl 2p, which is an impurity derived from the precursor salt ($SnCl_2.2H_2O$) employed to synthesize the SnO_2. Additionally, the FTIR spectrum (Figure S5) demonstrated the presence of some impurities related to carbonic groups (-CH). Therefore, the low performance of nanosized SnO_2 can in principle be attributed to the presence of these impurities. On the other hand, the sample with the highest cathodic current does not necessarily achieve greater efficiency in CO_2 reduction, as the CO_2RR competes with the H_2 evolution reaction and electrode redox reactions.

To confirm the CO_2RR performance of the SnO_x-based electrodes, electrolysis experiments were carried out under galvanostatic conditions (Fig. 3), applying − 50 mA (or − 6.25 mA/cm^2) for 30 min. The microsized SnO_2 electrocatalyst required the lower potential to maintain a constant current (of ca. − 0.7 V, followed by SnO (of ca. − 1.0 V) and nanosized SnO_2 (of ca. − 1.4 V) in the electrocatalysts. Therefore, nanometric SnO_2 requires much more power consumption to keep the current constant, which is likely due to the presence of impurities on its surface as demonstrated by FTIR and XPS analyses (Figure S4 and S5).

The HPLC results showed that formic acid was the only product in the liquid phase (Table 1). The SnO electrode

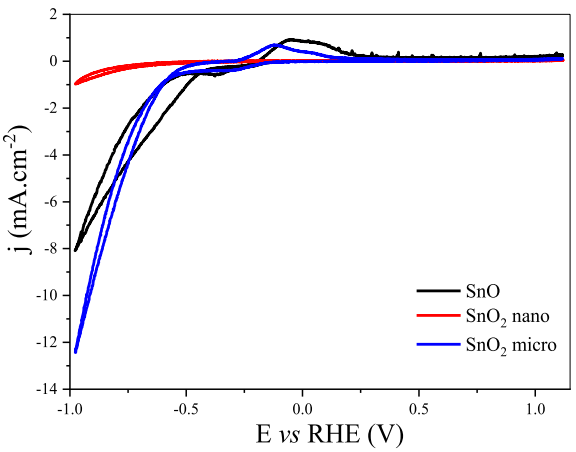

Figure 2: (a) Cyclic voltammetry in the electrolytic solution (0.5 M $KHCO_3$) performed with SnO_x-coated carbon fiber electrodes.

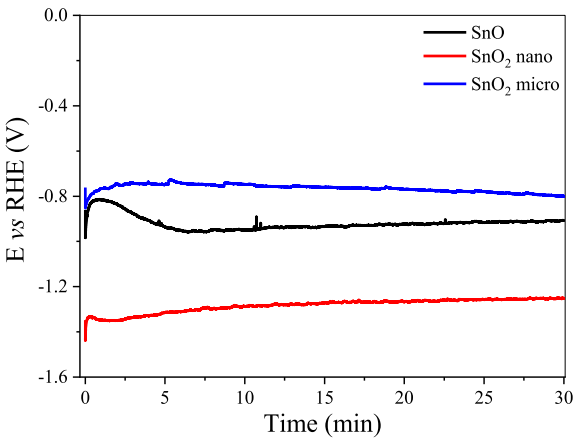

Figure 3: Electrolysis under galvanostatic conditions of − 50 mA during 30 min of SnO_x-based electrocatalysts.

TABLE 1: $HCOO^-$ concentration outputs and the FE (η) of the CO_2 reduction performed with SnO_x-based electrocatalysts under galvanostatic conditions (− 50 mA during 30 min).

	First cycle		Second cycle*	
Electrodes	[$HCOO^-$] (ppm)	η (%)	[$HCOO^-$] (ppm)	η (%)
Carbon fiber	0.7	0.2	–	–
SnO	215	46	290	61
Nano SnO_2	183	36	255	55
Micro SnO_2	106	22	201	42

*The second cycle was performed to evaluate the electrodes' stability.

© The Author(s) 2021

exhibited the highest performance in the $HCOO^-$ formation, followed by nanosized SnO_2 and microsized SnO_2. The uncoated fibers did not exhibit any catalytic activity in this reaction, indicating that SnO_x was the catalytically active site for CO_2RR. The different performances achieved by the SnO_x electrocatalysts indicate that the oxidation state of Sn, as well as the particle size, were both responsible for achieving significant CO_2RR performance profiles. The results suggest that the lower performance of SnO_2 electrodes compared to those of SnO can be related to the Sn^{4+} to Sn^{2+} competition reaction, as observed by CV analysis (Fig. 2). Nevertheless, the nanosized SnO_2 requires a reduction potential of approximately – 1.4 V in order to keep the current constant, whereas the microsized SnO_2 requires a reduction potential of about – 0.8 V. Therefore, the faradaic efficiency for nanosized SnO_2 could be higher due to the increase in the reduction potential, and not only because of the particle size, since it is well known that reduction potential influences directly on CO_2 reduction activity and selectivity. The Latimer diagram of Sn species around pH 7 showed that Sn^{4+} oxide should be reduced into Sn^{2+} oxide in a reduction potential around – 0.17 V vs RHE, while the Sn^{2+} oxide should be reduced into Sn metallic in a reduction potential around – 0.47 V vs RHE [27]. However, Dutta et al. [27] described the SnO_x's species stability under different electrochemical conditions, which was based on Pourbaix Diagram of Sn species and in operando Raman spectroscopy. They showed that the conversion of SnO_2 to metallic Sn requires more negative potentials than what could be predicted based on thermodynamic data, because the reduction of the SnO_2 is kinetically hindered. Therefore, both microsized SnO_2 and SnO are stable under galvanostatic conditions studied; however, the nanosized SnO_2 required a very high potential around – 1.4 V vs RHE to keep the – 50 mA. This catalyst should be partially converted into Sn^{2+} oxide and Sn metallic, it explains why the nanosized SnO_2 exhibited a higher faradaic efficiency than the microsized material.

To further understand the effects of particle size and reduction potential, we evaluated CO_2RR performance in potentiostatic conditions, i.e., by applying – 0.8 V over 3 h for nanosized and microsized SnO_2. It was observed that the microsized SnO_2 produced 789 ppm of formic acid, with a faradaic efficiency of 56%, whereas the nanosized SnO_2 achieved 21 ppm and an FE of 22%. Furthermore, microsized SnO_2 exhibited superior activity and selectivity for formic acid production. Again, this could reflect the impurities on the surface of nanosized SnO_2 electrocatalysts. This finding confirms the last experiment observation (galvanostatic), the reduction potential difference was the key to boosting the performance of the nanosized SnO_2.

In this step, the effect of the oxidation state of tin on the CO_2RR performance was evaluated. To attain this objective, we carried out a pre-reduction step in the SnO_2 electrodes by applying – 50 mA for 30 min under Ar purge in the same electrochemical cell. Then, the CO_2RR performance was evaluated under potentiostatic conditions, applying – 1.0 V for 2.5 h (Fig. 4). The obtained results were then compared with the performance of SnO_2 electrodes without any pre-reduction treatment (Table 2). It can be observed that the performance of SnO_2 electrocatalysts was enhanced following the pre-reduction step, and therefore this finding confirmed that the reduction of Sn^{4+} can compete with the CO_2 reduction and decrease the FE of formic acid formation. Additionally, we can confirm that Sn^{4+} is not the active site of the CO_2 reduction reaction. This corresponds to previously published data, for example, Lee et al. [38] showed that, under neutral conditions, metallic Sn is most likely the active site of CO_2RR. On the other hand, some authors have found that the Sn electrode possesses an oxide layer and shows excellent catalytic activity for CO_2 reduction, and that the Sn electrode removed its oxide layer, resulting in poor catalytic activity for CO_2 reduction, but with the hydrogen evolution reaction accelerating [23]. The results reported by Baruch et al. suggest that the active species for catalysis is an Sn^{2+} species rather than an Sn^{4+} one, as the first species can react with CO_2 to form the surface-bound carbonate, which is the intermediate products in the reduction of CO_2 to formate (Scheme S1). The first step of the reduction of CO_2 is preceded by a two-electron reduction of

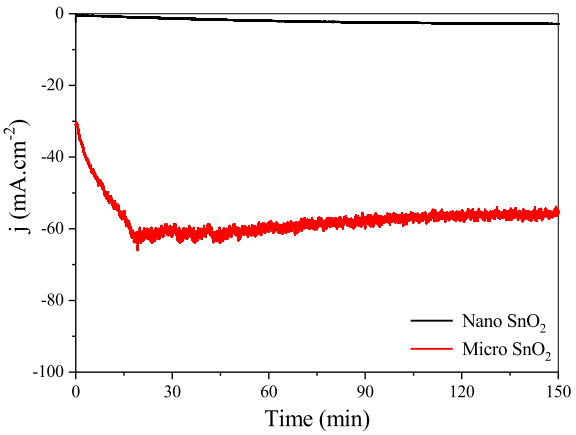

Figure 4: CO_2 reduction in 0.5 mol L^{-1} of $KHCO_3$ aqueous solution under potentiostatic conditions (– 1.0 V during 2.5 h) with microsized and nanosized SnO_2 electrodes following the pre-reduction step.

TABLE 2: $HCOO^-$ concentration outputs and FE (η) of CO_2 reduction performed with SnO_2 electrocatalysts with and without the pre-reduction (PR) step in potentiostatic conditions (– 1.0 V during 3 h).

Sample	[$HCOO^-$] (ppm)	η (%)
n-SnO_2	21	22
n-SnO_2 with PR	51	41
m-SnO_2	789	56
m-SnO_2 with PR	1711	60

© The Author(s) 2021

the electrode from a native SnO_2 to a Sn^{2+} oxyhydroxide, as described. Then CO_2 can react with this specie and forms the surface-bound carbonate, in the third step two electrons and a proton are transferred to the tin carbonate to form formate. Finally, the formate is quickly desorbed to return the surface to the Sn^{2+} oxyhydroxide surface [22]. It was demonstrated that CO_2 reduction overpotential is decreased by lowering the free energy of formation of carbonate [39]. These finding were confirmed by electrochemical experiments and DFT calculations [40]. Figure 4 shows a microsized SnO_2 electrocatalyst with a higher current density, production, and FE for formic acid formation than nanometric SnO_2.

The CO_2RR performance was evaluated at four different reduction potentials (– 0.2, – 0.6, – 0.8 and – 1.0 V), the polarization curves were obtained by average the current over a time period of 9000 s to each point, as is displayed in Fig. 5. It can be observed that when the reduction potential increased, the FE for formic acid formation was also enhanced. The increase in the reduction potential not only enhanced the current density/amount of formic acid formed but also increased the selectivity of the microsized SnO_2 electrocatalyst. This behavior is due to the H_2 evolution reaction, which exhibited a low reduction potential compared to that of the CO_2RR to formic acid [25].

The stability of the SnO_x-based electrodes was evaluated by means of two cycles of reuse under galvanostatic conditions, applying – 50 mA during 30 min (Table 1). It was verified for all SnO_x-based electrodes that, after the first cycle, the CO_2RR performance was increased. It can be observed that the increase in performance of the SnO_2 samples after the first cycle was more pronounced than for the SnO sample, likely due to the competition of the Sn^{4+}/Sn^{2+} reduction with the CO_2RR in the first cycle, this reaction may lead to a loss of the selectivity for formate production. This result corresponds to those observed in the pre-reduction experiment, i.e., after partial reduction of the SnO_2 electrodes, the catalytic activity was increased. To confirm the presence of the SnO_2 sample in the carbon fiber surface, even after two cycles of the CO_2RR experiment, an XRD and SEM analysis were performed on the micrometric SnO_2 (Fig. 6). The former showed that the crystalline SnO_2 phase did not change during the CO_2RR experiment; however, it was clear that the SnO_2 peaks decreased after the CO_2RR experiment. This peak decrease can be related to the Sn^{4+} reduction and/or its leaching into the solution. The SEM images showed that the morphology of microsized SnO_2 did not change during the CO_2RR; however, it could be verified that the SnO_2 particles became less agglomerated and more uniformly dispersed on the carbon fibers, which could relate to the surface reconstruction during CO_2RR operation, as observed in other studies [41–43]. Therefore, the enhanced CO_2RR performance after the first cycle could also be related to the better distribution of the SnO_2 particles across the carbon fiber surface.

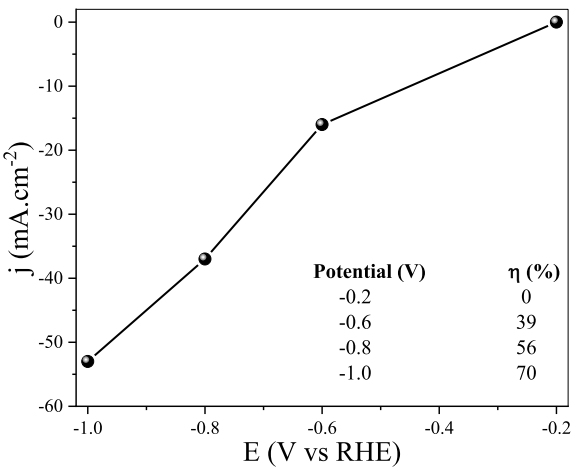

Figure 5: CO_2 reduction in 0.5 mol L^{-1} of $KHCO_3$ aqueous solution under potentiostatic conditions (– 0.6, – 0.8 and – 1.0 V for 2.5 h) with a micrometric SnO_2 electrode, after the pre-reduction step.

Conclusions

A simple, easy, and scalable method for impregnating SnO_x in carbon fibers was proposed in this study. All SnO_x electrodes were capable of converting CO_2 into formic acid, with a maximum FE of almost 70% for the SnO_2 catalyst. On the other hand, carbon fiber without tin oxide was not effective for the CO_2 reduction reaction. It was demonstrated that both the particle size and oxidation state played an important role in the CO_2RR performance. The SnO electrocatalyst exhibited high activity for CO_2RR compared to SnO_2 electrocatalysts, likely due to the requirement of reducing Sn^{4+}. Nanosized SnO_2 exhibited a low CO_2 reduction performance due to the impurities on this material surface, as demonstrated by FTIR and XPS analysis. The pre-reduction step for both SnO_2 electrodes increased their CO_2RR performance, indicating that Sn^{2+} is the active site under potentiostatic conditions, and the microsized SnO_2 electrode showed greater efficiency in the generation of formic acid. The CO_2 reduction mechanism on the SnO_x surface was proposed based on our results and in the literature. The increase in the reduction potential increased the CO_2RR conversion of formic acid selectivity of the micrometric SnO_2 electrocatalyst. The results showed that the oxide remained on the surface, and therefore it constitutes a stable surface for reactions.

© The Author(s) 2021

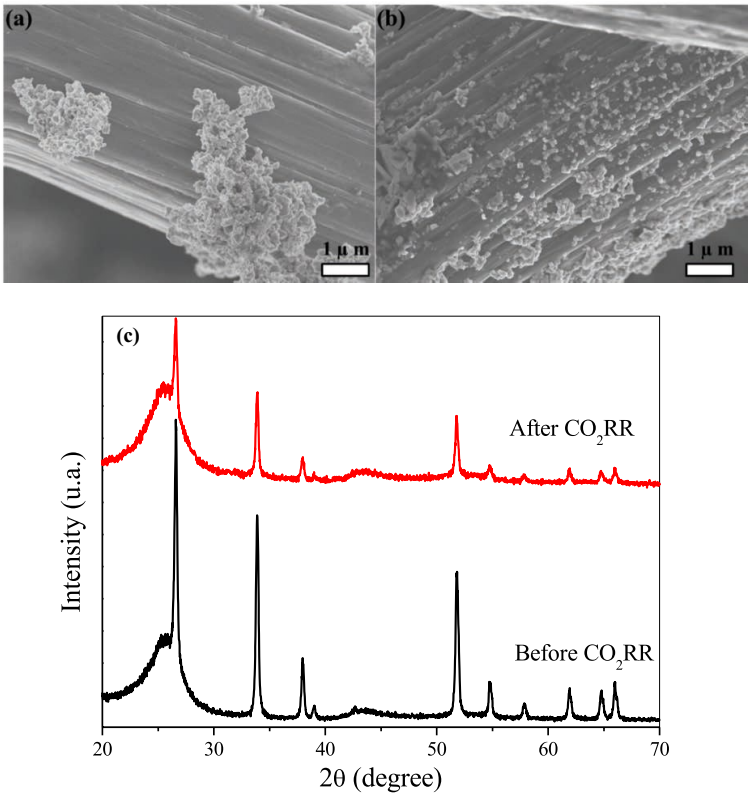

Figure 6: SEM images of the micrometric SnO_2 electrode, (a) before and (b) after CO_2RR. (c) XRD pattern of the micrometric SnO_2 electrode before and after CO_2RR.

Methodology

Preparation and characterization of SnO_x-based electrodes

A general procedure was used to deposit the SnO_x catalyst ink on the carbon fibers. To obtain the catalyst ink, 18 mg of SnO_x with Nafion (5% w/w) was dispersed in 2 mL of isopropanol, using sonication. The catalyst/Nafion ratio was 90:10 (wt:wt), respectively. The mixture was dried in a fume hood and then deposited to the carbon fiber electrode (area of 8 cm^2) by means of brushing. The electrodes were then cured at 80 °C for 1 h. Three different SnO_x-based materials were evaluated: (i) microsized SnO_2 (99.9%, Sigma-Aldrich); (ii) microsized SnO (99.99%, Sigma-Aldrich); and (iii) nanosized SnO_2 that was prepared by means of hydrothermal treatment, as described elsewhere [33]. In detail, 0.564 g of $SnCl_2.2H_2O$ (Sigma-Aldrich) was dissolved in 100 mL of ethanol anhydrous (99.5% purity, Dinâmica) and then under vigorous stirring, 22.5 mL of distilled water was added dropwise at room temperature for 12 h. After that, the suspension was cleaned by dialysis in 5 L of distilled water, often renewed, until removing all chloride ions, which was confirmed by tests with $AgNO_3$ solution (0.1 mol L^{-1}). Then, the solution inside the dialysis bag was dried at 70 °C for 12 h, ground with an agate mortar. After that, the as-prepared sample was treated hydrothermally up to 200 °C for 4 h. The concentrations of the SnO_x investigated (2.2 mg cm^{-2}) were chosen on the basis of previous reports [26, 44, 45]. The samples were characterized by X-ray diffraction (XRD) at $2\theta = 10°$ to 70°, using a monochromatized X-ray beam from nickel-filtered Cu kα radiation ($\lambda = 0.15406$ nm, 30 kV, 30 mA—Rigaku Multiflex-Ultima IV). The morphological properties of the samples were characterized using a scanning electron microscope (SEM, JEOL JSM 670F) operating at 5 kV (secondary electron detector) at different magnifications. A Fourier Transform Infrared spectrometer (FTIR) (Bruker VERTEX 70) was used to investigate surface changes using nanosized SnO_2-containing KBr disks with 64 scans and 4 cm^{-1} resolution in the 4000–400 cm^{-1}. X-ray photoelectron spectroscopy (XPS) analyses were performed on a Scienta Omicron, model ESCA$^+$ spectrometer using monochromatic AlKα (1486.6 eV) radiation. Peak decomposition was performed using a Gaussian–Lorentzian line shape with a Shirley nonlinear sigmoid-type baseline. The binding energies were corrected for charging effects by assigning a value of 284.8 eV to the adventitious C 1s line. The data were analyzed using CasaXPS software (Casa Software Ltd., U.K.). N_2 adsorption–desorption isotherms were recorded on a Micromeritics ASAP 2020 analyzer at 77 K. Samples were previously degassed at 80 °C under vacuum until a degassing pressure, 10 µmHg. The Brunauer–Emmett–Teller (BET) method was used to calculate the SSA (S_{BET}).

© The Author(s) 2021

Evaluation of CO_2 reduction performance

The CO_2 reduction reaction experiments were studied in a two-chamber electrochemical cell, separated by a proton exchange membrane (Nafion 117) in an aqueous $KHCO_3$ (0.5 mol L^{-1}) solution. The electrolyte was saturated with CO_2 (pH 6.9) for 30 min prior to each measurement. The SnO_x-coated carbon fiber electrode was used as the working electrode, and a Pt mesh and Ag/AgCl electrode were used as the counter and reference electrodes, respectively. All of the potentials presented herein were converted to the RHE reference scale using the following equation: E (*vs* RHE) = E (*vs* Ag/AgCl) + 0.210 V + 0.0591*pH. The electrochemical measurements were carried out using a Potentiostat/Galvanostat (Model 273, Princeton Applied Research).

These cyclic voltammetric measurements were performed from 1.1 to − 1.0 V. The measurements were conducted in order to verify the regions where the reactions of interest occurred. The performance of the SnO_x-based catalysts was evaluated under galvanostatic conditions, applying a current of − 0.05 A for 30 min. The stability of the catalysts was evaluated by two reuse cycles of galvanostatic experiments. The species produced by the reduction of CO_2 in the liquid phase were analyzed by high-performance liquid chromatography (HPLC) in order to calculate the FE (%) of the process. The sample was collected in the cathode compartment of the electrochemical cell following the CO_2 reduction reaction and injected into the chromatograph (HPLC-LC-20AD, Shimadzu) with an Aminex HPX-87H column (300 × 7.8 mm) capable of analyzing carboxylic acids and alcohols. A diluted solution of H_2SO_4 (3.3 mmol L^{-1}) was used as the mobile phase with a flow rate of 0.6 mL min^{-1}. A sample volume of 20 µL was injected into the column loop. The column and detectors were kept at 40 °C. The chromatograph was equipped with a differential refractive index detector (RID-10A) that is suitable for the detection of alcohols, and a UV–Vis detector (SPD-20A, deuterium lamp, λ = 210 nm), which is suitable for the analysis of carboxylic acids. Data obtained by HPLC were used to calculate the Faradaic efficiency (FE) of the CO_2 electrochemical reduction in relation to formation of formate ($HCOO^-$). The Faradaic efficiency (FE) of the CO_2 electrochemical reduction of products was calculated as

$$FE = \frac{n \times F \times n_{HCOO-}}{Q} \times 100\%$$

where n represents the number of electrons transferred from CO_2 for the production of one molecule of formate, F is the Faraday constant, n_{HCOO^-} is the number of moles of the formate, and Q is the total charge. In this case, $n = 2$; F is Faraday's constant (96 485 C mol^{-1} of electrons); n_{HCOO^-} is calculated by HPLC measurements.

To evaluate the effect of Sn oxidation state, it was performed a pre-reduction step in the same electrochemical cell in both SnO_2 nanosized and microsized, i.e., a current of − 0.05 A was applied for 30 min under an Ar purge in order to reduce the species of Sn^{4+}; then, an experiment was performed under potentiostatic conditions, with − 0.8 V applied for 2.5 h. The performance of both electrodes was compared with and without this pre-treatment, to investigate the Sn site active. Additionally, the effect of the reduction potential (− 0.2 to − 1.0 V) on the FE of the microsized SnO_2 was also analyzed after the same pre-reduction step.

Acknowledgments

The authors acknowledge FAPESP (São Paulo Research Foundation) for the scholarships (Grants: #17/09713-0, #16/09746-3, #2019/22183-6) and financial support (Grant #13/16930-7), CNPq (Conselho Nacional de Desenvolvimento Científico e Tecnológico) for the financial support (Grants #304458/2013-9, #407497/2018-8, #17-12437-5). The authors would like to thank Prof. Valmor R. Mastelaro for XPS experiments, Dr. Gelson T. S. T. da Silva for FTIR and N_2 physisorption experiments and Dr. Valdecir A. Paganin for the fruitful discussions and general assistance. Osmando F. Lopes also acknowledges Alexander von Humboldt Foundation and CAPES by Post-Doc Research Fellowship (CAPES/Humboldt Agreement—Process 88881.368050/2019-01).

Funding

Open Access funding enabled and organized by Projekt DEAL.

Data Availability

All data generated or analyzed during this study are included in this published article (and its supplementary information files).

Declarations

Conflict of interest On behalf of all authors, the corresponding author states that there is no conflict of interest.

Supplementary Information

The online version contains supplementary material available at https://doi.org/10.1557/s43578-021-00250-1.

Open Access

This article is licensed under a Creative Commons Attribution 4.0 International License, which permits use, sharing, adaptation, distribution and reproduction in any medium or format,

© The Author(s) 2021

as long as you give appropriate credit to the original author(s) and the source, provide a link to the Creative Commons licence, and indicate if changes were made. The images or other third party material in this article are included in the article's Creative Commons licence, unless indicated otherwise in a credit line to the material. If material is not included in the article's Creative Commons licence and your intended use is not permitted by statutory regulation or exceeds the permitted use, you will need to obtain permission directly from the copyright holder. To view a copy of this licence, visit http://creativecommons.org/licenses/by/4.0/.

References

1. J. Wu, Y. Huang, W. Ye, Y. Li, CO_2 reduction: from the electrochemical to photochemical approach. Adv. Sci. **4**(11), 1 (2017)
2. N.S. Lewis, D.G. Nocera, Powering the planet: chemical challenges in solar energy utilization. Proc. Natl. Acad. Sci. USA **103**(43), 15729 (2006)
3. M. Gattrell, N. Gupta, A. Co, A review of the aqueous electrochemical reduction of CO_2 to hydrocarbons at copper. J. Electroanal. Chem. **594**(1), 1 (2006)
4. F.P. García de Arquer, C.T. Dinh, A. Ozden, J. Wicks, C. McCallum, A.R. Kirmani, D.H. Nam, C. Gabardo, A. Seifitokaldani, X. Wang, Y.C. Li, F. Li, J. Edwards, L.J. Richter, S.J. Thorpe, D. Sinton, E.H. Sargent, CO_2 electrolysis to multicarbon products at activities greater than 1 A cm^{-2}. Science **367**(6478), 661 (2020)
5. S. Garg, M. Li, A.Z. Weber, L. Ge, L. Li, V. Rudolph, G. Wang, T.E. Rufford, Advances and challenges in electrochemical CO_2 reduction processes: an engineering and design perspective looking beyond new catalyst materials. J. Mater. Chem. A **8**(4), 1511 (2020)
6. M.G. Kibria, J.P. Edwards, C.M. Gabardo, C.T. Dinh, A. Seifitokaldani, D. Sinton, E.H. Sargent, Electrochemical CO_2 reduction into chemical feedstocks: from mechanistic electrocatalysis models to system design. Adv. Mater. **31**(31), 1 (2019)
7. G. Gurudayal, J. Bullock, D.F. Srankó, C.M. Towle, Y. Lum, M. Hettick, M.C. Scott, A. Javey, J. Ager, Efficient solar-driven electrochemical CO_2 reduction to hydrocarbons and oxygenates. Energy Environ. Sci. **10**, 2222 (2017)
8. C. Kim, H.S. Jeon, T. Eom, M.S. Jee, H. Kim, C.M. Friend, B.K. Min, Y.J. Hwang, Achieving selective and efficient electrocatalytic activity for CO_2 reduction using immobilized silver nanoparticles. J. Am. Chem. Soc. **137**(43), 13844 (2015)
9. S. Liang, N. Altaf, L. Huang, Y. Gao, Q. Wang, Electrolytic cell design for electrochemical CO_2 reduction. J. CO2 Util. **35**(August 2019), 90 (2020)
10. G.T.S. Silva, O.F. Lopes, E.H. Dias, J.A. Torres, A.E. Nogueira, L.A. Faustino, F.S. Prado, A.O.T. Patrocínio, C. Ribeiro, Redução de CO_2 em Hidrocarbonetos e Oxigenados: Fundamentos Estratégias e Desafios. Quim. Nova (2021). https://doi.org/10.21577/0100-4042.20170745
11. R. Kortlever, J. Shen, K.J.P. Schouten, F. Calle-Vallejo, M.T.M. Koper, Catalysts and reaction pathways for the electrochemical reduction of carbon dioxide. J. Phys. Chem. Lett. **6**(20), 4073 (2015)
12. S. Liu, J. Xiao, X.F. Lu, J. Wang, X. Wang, X.W. Lou, Efficient electrochemical reduction of CO_2 to HCOOH over Sub-2 nm SnO_2 quantum wires with exposed grain boundaries. Angew. Chemie **58**(25), 8499 (2019)
13. L.G. Puppin, M. Khalid, G.T.T. Da Silva, C. Ribeiro, H. Varela, O.F. Lopes, Electrochemical reduction of CO_2 to formic acid on $Bi_2O_2CO_3$/carbon fiber electrodes. J. Mater. Res. **35**(3), 272 (2020)
14. B. Kumar, M. Llorente, J. Froehlich, T. Dang, A. Sathrum, C.P. Kubiak, Photochemical and photoelectrochemical reduction of CO_2. Annu. Rev. Phys. Chem. **63**, 541 (2012)
15. E.E. Benson, C.P. Kubiak, A.J. Sathrum, J.M. Smieja, Electrocatalytic and homogeneous approaches to conversion of CO_2 to liquid fuels. Chem. Soc. Rev. **38**(1), 89 (2009)
16. R. Reske, H. Mistry, F. Behafarid, B.R. Cuenya, P. Strasser, Particle size effects in the catalytic electroreduction of CO_2 on Cu nanoparticles. J. Am. Chem. Soc. **136**(19), 6978 (2014)
17. H. Mistry, A.S. Varela, C.S. Bonifacio, I. Zegkinoglou, I. Sinev, Y.W. Choi, K. Kisslinger, E.A. Stach, J.C. Yang, P. Strasser, B.R. Cuenya, Highly selective plasma-activated copper catalysts for carbon dioxide reduction to ethylene. Nat. Commun. **7**, 12123 (2016)
18. O.F. Lopes, H. Varela, Effect of annealing treatment on electrocatalytic properties of copper electrodes toward enhanced CO_2 reduction. ChemistrySelect **3**(31), 9046 (2018)
19. S. Zhu, T. Li, W. Bin Cai, M. Shao, CO_2 electrochemical reduction as probed through infrared spectroscopy. ACS Energy Lett. **4**(3), 682 (2019)
20. M.B. Ross, P. De Luna, Y. Li, C.T. Dinh, D. Kim, P. Yang, E.H. Sargent, Nat. Catal. **2**, 648 (2019)
21. K. Bejtka, J. Zeng, A. Sacco, M. Castellino, S. Hernández, M.A. Farkhondehfal, U. Savino, S. Ansaloni, C.F. Pirri, A. Chiodoni, Chainlike mesoporous SnO_2 as a well-performing catalyst for electrochemical CO_2 reduction. ACS Appl. Energy Mater. **2**(5), 3081 (2019)
22. M.F. Baruch, J.E. Pander, J.L. White, A.B. Bocarsly, Mechanistic insights into the reduction of CO_2 on tin electrodes using in situ ATR-IR spectroscopy. ACS Catal. **5**(5), 3148 (2015)
23. R. Zhang, W. Lv, L. Lei, Role of the oxide layer on Sn electrode in electrochemical reduction of CO_2 to formate. Appl. Surf. Sci. **356**, 24 (2015)
24. S. Zhang, P. Kang, T.J. Meyer, Nanostructured tin catalysts for selective electrochemical reduction of carbon dioxide to formate. J. Am. Chem. Soc. **136**(5), 1734 (2014)

© The Author(s) 2021

25. Y. Hori: CO_2-reduction, catalyzed by metal electrodes. In Vielstich, W., Lamm, A., Gasteiger, H.A., Yokokawa, H (eds.) Handbook of Fuel Cells (2010). https://doi.org/10.1002/9780470974001.f207055
26. S. Lee, J.D. Ocon, Y. Il Son, J. Lee, Alkaline CO_2 electrolysis toward selective and continuous HCOO-production over SnO_2 nanocatalysts. J. Phys. Chem. C **119**(9), 4884 (2015)
27. A. Dutta, A. Kuzume, M. Rahaman, S. Vesztergom, P. Broekmann: Monitoring the chemical state of catalysts for CO_2 electroreduction: an in operando study. ACS Catal. **5**(12), 7498 (2015)
28. Y. Chen, M.W. Kanan, Tin oxide dependence of the CO_2 reduction efficiency on tin electrodes and enhanced activity for tin/tin oxide thin-film catalysts. J. Am. Chem. Soc. **134**(4), 1986 (2012)
29. C.W. Li, M.W. Kanan, CO_2 reduction at low overpotential on Cu electrodes resulting from the reduction of thick Cu_2O films. J. Am. Chem. Soc. **134**(17), 7231 (2012)
30. A. Del Castillo, M. Alvarez-Guerra, J. Solla-Gullón, A. Sáez, V. Montiel, A. Irabien, Electrocatalytic reduction of CO_2 to formate using particulate Sn electrodes: effect of metal loading and particle size. Appl. Energy **157**, 165 (2015)
31. W. Xu, D. Du, R. Lan, J. Humphreys, D.N. Miller, M. Walker, Z. Wu, J.T.S. Irvine, S. Tao, Electrodeposited NiCu bimetal on carbon paper as stable non-noble anode for efficient electrooxidation of ammonia. Appl. Catal. B Environ. **237**, 1101 (2018)
32. E. Antolini, Carbon supports for low-temperature fuel cell catalysts. Appl. Catal. B Environ. **88**(1–2), 1 (2009)
33. A. Juliana, A. Torres, G.T.S.T. Silva, F.B.D.F. Silva, C. Ribeiro, Experimental evidence of CO_2 photoreduction activity of SnO_2 nanoparticles. ChemPhysChem (2020). https://doi.org/10.1002/cphc.202000786
34. J. Albo, A. Irabien, Cu_2O-loaded gas diffusion electrodes for the continuous electrochemical reduction of CO_2 to methanol. J. Catal. **343**, 232 (2016)
35. E. Andrews, M. Ren, F. Wang, Z. Zhang, P. Sprunger, R. Kurtz, J. Flake, Electrochemical reduction of CO_2 at Cu nanocluster/$(10\bar{1}0)$ ZnO electrodes. J. Electrochem. Soc. **160**(11), H841 (2013)
36. A.M.S. El Din, F.M.A. El Wahab, On the anodic passivity of tin in alkaline solutions. Electrochim. Acta **9**(7), 883 (1964)
37. S.D. Kapusta, N. Hackerman, Anodic passivation of tin in slightly alkaline solutions. Electrochim. Acta **25**(12), 1625 (1980)
38. M.Y. Lee, S. Ringe, H. Kim, S. Kang, Y. Kwon, Electric field mediated selectivity switching of electrochemical CO_2 reduction from formate to CO on carbon supported Sn. ACS Energy Lett. **5**(9), 2987 (2020)
39. Z.M. Detweiler, J.L. White, S.L. Bernasek, A.B. Bocarsly, Anodized indium metal electrodes for enhanced carbon dioxide reduction in aqueous electrolyte. Langmuir **30**(25), 7593 (2014)
40. G.B. Damas, C.R. Miranda, R. Sgarbi, J.M. Portela, M.R. Camilo, F.H.B. Lima, C.M. Araujo, On the mechanism of carbon dioxide reduction on sn-based electrodes: insights into the role of oxide surfaces. Catalysts (2019). https://doi.org/10.3390/catal9080636
41. W. Luo, Q. Zhang, J. Zhang, E. Moioli, K. Zhao, A. Züttel, Electrochemical reconstruction of ZnO for selective reduction of CO_2 to CO. Appl. Catal. B Environ. **273**(April), 119060 (2020)
42. P. Liu, H. Liu, S. Zhang, J. Wang, C. Wang, Significant role of reconstructed character on CuO-derived catalyst for enhanced electrocatalytic reduction of CO_2 to multicarbon products. Electrochim. Acta **354**, 136753 (2020)
43. S. Song, J. Meng, Y. Wang, J. Zhou, L. Zhang, N. Gao, C. Guan, G. Xiao, Z. Hu, H.J. Lin, C. Te Chen, X.L. Du, J. Hu, J.Q. Wang, Molten salt treated Cu foam catalyst for selective electrochemical CO_2 reduction reaction. ChemistrySelect **5**(38), 11927 (2020)
44. B. Kumar, V. Atla, J.P. Brian, S. Kumari, T.Q. Nguyen, M. Sunkara, J.M. Spurgeon, Reduced SnO_2 porous nanowires with a high density of grain boundaries as catalysts for efficient electrochemical CO_2-into-HCOOH conversion. Angew. Chemie Int. Ed. **56**(13), 3645 (2017)
45. A. Del Castillo, M. Alvarez-Guerra, J. Solla-Gullón, A. Sáez, V. Montiel, A. Irabien, Sn nanoparticles on gas diffusion electrodes: synthesis, characterization and use for continuous CO_2 electroreduction to formate. J. CO2 Util. **18**, 222 (2017)

© The Author(s) 2021